

# A VLSI-Oriented Continuous-Time CNN Model

*S. Espejo, R. Carmona, R. Domínguez-Castro and A. Rodríguez-Vázquez*

Instituto de Microelectrónica de Sevilla - Centro Nacional de Microelectrónica  
Avda. Reina Mercedes s/n, (Edif. CICA)  
E-41012, Sevilla, Spain

*International Journal of Circuit Theory and Applications,*  
*Vol. 24, pp. 341-356, May-June 1996.*

© 1996 Ed. Wiley. Personal use of this material is permitted. However, permission to reprint/republish this material for advertising or promotional purposes or for creating new collective works for resale or redistribution to servers or lists, or to reuse any copyrighted component of this work in other works must be obtained from the Ed. Wiley.

This material is presented to ensure timely dissemination of scholarly and technical work. Copyright and all rights therein are retained by authors or by other copyright holders. All persons copying this information are expected to adhere to the terms and constraints invoked by each author's copyright. In most cases, these works may not be reposted without the explicit permission of the copyright holder.

# A VLSI-Oriented Continuous-Time CNN Model

*S. Espejo, R. Carmona, R. Domínguez-Castro and A. Rodríguez-Vázquez*

Centro Nacional de Microelectrónica-Universidad de Sevilla  
Edificio CICA, C/Tarfia s/n, 41012-Sevilla, SPAIN  
Phone: +34 - 5 - 423 99 23. Fax: +34 - 5 - 462 45 06. E-mail: espejo@cnm.us.es

## Abstract

This paper presents an analysis of the stability and convergence properties of the Full Signal Range CNN model. These properties are demonstrated to be similar to those of the Chua-Yang's model, and the I/O mapping of known applications is shown to be unaffected by the modification introduced in this new model. In this modified CNN model, the dynamic range of the cell state-variables equals the dynamic range of the cell output variables, and is invariant with the application. This feature results in simpler circuit implementations, thus allowing higher cell densities and improving the robustness of CNN integrated circuits. In particular the Full Signal Range CNN model is specially well-suited for programmable CNN integrated circuits with binary outputs.

### Front-Page Footnotes:

- 1
- 2

---

1. Part of this research has been reported in the Proceedings of the 1994 Int. Workshop on Cellular Neural Networks and their Applications, held in Rome [17].
2. Research of Ricardo Carmona has been partially supported by IBERDROLA, S.A. under contract INDES-94/377.

# A VLSI-Oriented Continuous-Time CNN Model

*S. Espejo, A. Rodríguez-Vázquez, R. Domínguez-Castro, and R. Carmona*

## I. INTRODUCTION

Analog microelectronic circuits are inherently parallel, have larger area and power efficiency than digital counterparts, and enable direct interface to sensory devices [1]. These features render them very well suited for hardware implementation of Cellular Neural Networks (CNN), and have motivated several authors to explore them [2], [3], [4], [5], [6]. Some used the cell model proposed by Chua and Yang [7], [8], which contains a linear loss term per cell and whose non-linearity is only at the output function, while others have considered a generalization with non-linearities in the local losses as well [9],

$$\tau \frac{dx^c}{dt} = -g_m(x^c) + \sum_{d \in N(c)} a_d^c y^d + \sum_{d \in N(c)} b_d^c u^d + d^c \quad (1)$$

where,

$$y^c = f(x^c) = \begin{cases} 1, & \forall x^c \geq 1 \\ x^c, & \forall |x^c| < 1 \\ -1, & \forall x^c \leq -1 \end{cases} \quad ; \quad g_m(x^c) = \begin{cases} m(x^c - 1) + 1 & \forall x^c > 1 \\ x^c & \forall |x^c| \leq 1 \\ m(x^c + 1) - 1 & \forall x^c < -1 \end{cases} \quad (2)$$

and the notation used for the interactions among cells follows the convention in [10] -- not included here.

This model was first proposed by the authors in [9], where they considered the limiting case of  $m \rightarrow \infty$  and consequently, cell state variables are restricted to the same variation interval as input and output variables,  $[-1, 1]$ . This differs significantly from Chua-Yang's model, where the interval for state variables is larger and its amplitude varies with the values of the templates. In the new model the state and the output variables of each cell merge for all practical purposes, the block that realizes the output non-linearity is discarded, and the complexity of the associated circuitry decreases<sup>3</sup>. Consequently, it yields larger cell density and smaller power consumption than the original model -- prerequisites to increase complexity in the production of CNN chips. In addition, it is insensitive to uniform variations of CNN coefficients, an important feature in a VLSI context, where process parameters are always subject to variations. Finally, for a given time constant, the processing speed is approximately doubled in common applications.

This paper aims to provide an analysis of stability and convergence properties of this new model,

---

3. These considerations are somewhat dependent on technology and circuit design style. [9] demonstrates their validity for current-mode circuits, where the non-linear loss term exploits intrinsic device non-linearities while rendering these losses linear requires extra linearization circuitry. Similar considerations apply for  $g_mC$  and MOSFETC styles as well [12].

denominated hereinafter as the Full Signal Range (FSR) model. This analysis will be carried out for convenience and completeness on the  $m$ -parameter family of (1)-(2), referred to as the Improved Signal Range (ISR). Section II first provides an intuitive derivation of the FSR model based on the circuit simplification objective, and then introduces the ISR as the result of a gradual transition from the Chua-Yang's to the FSR. Section III demonstrates the basic stability and convergence results for the models in this family, including those initially reported for the original model in [7] and [8]. Section IV discusses the mathematical formulation of the modified model obtained as a limit case of the previous family of models, and compares it with that predicted by the circuit derivation in Section II. Finally, Section V contains a summary and the conclusions.

## II. THE IMPROVED SIGNAL RANGE FAMILY OF CNN MODELS

### A. Transition from the Chua-Yang Model to the FSR Model.

Fig. 1 shows a block diagram of a CNN cell based on Chua-Yang's model, which corresponds to using  $m = 1$  in the left-hand side equation in (2). Each cell receives/generates a weighted contribution from/for each cell in its neighborhood. Incoming contributions are added directly at the input of the cell and integrated. The output of the integrator represents the state variable  $x^c(t)$ , which is fed-back to the input with a scaling factor  $-1$  that represents a normalization factor for the rest of the weights. A nonlinear block is then used to generate the output  $y^c(t)$ , which is replicated and scaled to generate the out-coming contributions for the cells in the neighborhood. The implementation of the control and the offset terms is not shown since this part of the cell performs a static function, and is irrelevant in the discussion of the modified model.

Variables  $x^c(t)$  and  $y^c(t)$  in Fig. 1 are identical while the cell is within its linear region. Otherwise,  $y^c(t)$  saturates at  $\pm 1$  (after normalization), while  $x^c(t)$  goes beyond these limits. Any correct circuit implementation must provide room for these larger variations of the state variable, which means that the output signal range of the integrator must be wide enough. The required signal range, normalized to that of the output variable is given by [8],

$$S^c = 1 + \sum_{d \in N(c)} [ |a_d^c| + |b_d^c| ] + |d^c| \quad (3)$$

where it is assumed that the cells' initial condition and input are restricted to the unitary interval, that is,  $|x^c(0)| \leq 1$  and  $|u^c| \leq 1$ . The value of  $S^c$  is between 4 and 20 for most reported applications [11]. This enlargement of the state variable range represents increased complexity in the circuitry used to implement the cell. Particularly, for programmable CNNs, the dependence of  $S^c$  on the CNN coefficients forces either the use of a fixed high value for  $S^c$  valid for arbitrary templates, or the possibility to change the normalization parameter through the inclusion of a programmable-saturation nonlinear block in Fig. 1. Either approach results in increased circuit complexity and/or accuracy requirements. In addition, the scaling block used to realize the loss term (the negative feedback block with weight  $-1$  in Fig. 1) must be designed with an input signal-range larger than that of the scaling blocks used to generate the feedback-template contributions. The use of different circuitry to realize both types of

scaling blocks represents an additional difficulty in accurate matching of the CNN coefficients with respect to the loss term.

These considerations motivate searching for alternative models. To this end, note the output variable  $y^c(t)$  contains all the static information interchanged between cells. In addition, for applications where the output is binary<sup>4</sup> [8], [10], [11] this variable contains all the relevant output information from the network. From a dynamic point of view, the actual value of the state variable beyond the limits of the linear region can be considered as a measure of the inertia of the output variable to remain saturated. Although one may think a priori of this feature as significant for the input/output mapping of a CNN, it is heuristically observed that this is not actually the case for most applications. Hence, from a functional point of view, it appears that  $x^c(t)$  may be restricted to the unitary interval as well and that the state and output variables may be merged into a single one with no influence on the functionality. This is actually the idea behind the FSR model, whose block diagram is depicted in Fig. 2. The main modification centers on the integrator, which in Fig. 1 is designed with sufficient output-signal range to avoid its saturation during the dynamic evolution of the cell, while in Fig. 2 it is designed to have saturation limits equal to those of the output variable. Thus, this block responds to the usual integral law while its output  $z^c(t)$  (modified state variable) is within its saturation limits ( $\pm 1$  after normalization). Whenever the state variable reaches  $+1$  (alternatively  $-1$ ), it remains clamped to this value as long as the input of the integrator is non-negative (alternatively non-positive), without modifying its value and hence without accumulating inertia: as soon as the integrator input becomes negative (alternatively positive), the modified state variable will enter the linear region again. Fig. 3 shows a conceptual block diagram to realize this behavior through electronic circuits. Analysis of Fig. 2 using the integrator of Fig. 3 obtains,

$$\tau \frac{dz^c}{dt} = \begin{cases} 0 & , \text{if } [(|z^c| = 1) \text{ and } (\text{sgn}(z^c) = \text{sgn}(h^c))] \\ h^c & , \text{otherwise} \end{cases} \quad (4)$$

where  $\text{sgn}(\bullet)$  is the sign function and,

$$a_d^c = \begin{cases} a_d^c - 1 & , c = d \\ a_d^c & , c \neq d \end{cases} \quad h^c = \sum_{d \in N(c)} a_d^c z^d + \sum_{d \in N(c)} b_d^c u^d + d^c \quad (5)$$

which corresponds to the limiting case of  $m \rightarrow \infty$  in (1)-(2) with  $z^c(t) \equiv x^c(t) \equiv y^c(t)$ . Thus, there is now only one signal-node and its signal range is  $[-1, 1]$  independent of the template coefficients. Besides, all the scaling blocks in Fig. 2 are realized with the same type of circuitry, facilitating their design and matching. In summary, the FSR circuitry is simpler and more robust than Chua-Yang's<sup>5</sup>.

---

4. Binary Output was assumed in the model proposed originally by Chua and Yang. Also, the majority of applications of CNNs have binary output.

5. In the above formulation, we assume that  $|z^c| \leq 1$  at every time instant. This is in fact direct consequence of the definition of the time derivative of  $z^c(t)$  in the unitary interval, which ensures that it will never go beyond  $\pm 1$  if it is initially inside. In a real implementation, however, it must be ensured that the value of the derivative when  $|z^c| > 1$  tends to restore the state variable towards the unitary interval.

### B. A Gradual Transition from the Chua-Yang to the FSR: The Improved Signal Range Model.

To establish a connection among the mathematical formulations of the original and the FSR models, we consider it convenient to use the  $m$ -parameter ISR family of models given in (1)-(2), instead of directly the FSR model. Fig. 4 shows the block diagram of this family, where the feedback template elements are not redefined and the cell output is still related to the state variable by the usual relationship in (2). Hence, the only difference between this and the original model is the modification of the loss term. Note that if  $m = 1$ , then  $g_m(x^c) = x^c$  resulting in the original CNN model. On the other hand, when  $m \rightarrow \infty$  the infinite losses in the saturation regions limit the state variable to the unitary interval, resulting in the FSR model. This is further discussed in Section IV.

The similarity between the Chua-Yang and ISR models allows using procedures as in [8] and [10] to demonstrate some stability and convergence properties of the ISR model family. All the results will be applicable to both the original and the FSR models, since they are particular cases of the ISR family.

## III. STABILITY AND CONVERGENCE PROPERTIES OF ISR CNN MODELS

This section is written in the form of statements and proofs. Except where explicitly stated, the statements are valid independent of the feedback and control templates, offset terms, and boundary conditions (including non-uniform networks). They are also valid for any set of initial states and cell inputs (with no restriction on the unitary interval). The only assumption made is that the network coefficients, initial states, and cell input are finite.

Boundary conditions are not considered in the following demonstrations. However, the networks considered are finite (limited number of cells), and the effects of boundary conditions on border cells can be included redefining their offset terms, and considering zero feedback and control templates for boundary cells<sup>6</sup>. If reciprocity is considered a condition, the corresponding feedback and control template elements of border cells can also be set to zero without affecting the network.

For convenience, we include the following definitions:

$$k^c \equiv \sum_{d \in N(c)} b_d^c u^d + d^c \quad (6)$$

which contains all the time-invariant contributions to each individual cell, and

$$M^c \equiv \sum_{d \in N(c)} |a_d^c| + |k^c| \quad (7)$$

which is a measure of the maximum absolute value of the contributions to a particular cell (excluding its loss term). For simplicity, we will assume that  $M^c \geq 1$ , which is the most common case (for instance, whenever  $a_c^c \geq 1$ ). This assumption is not necessary for any of the following statements [12].

---

6. Border cells are CNN cells located on the border of the array, which respond to the same dynamic equation as the remaining inner cells. Boundary cells are located in the surroundings of the array, and have time-invariant state variables. Their purpose is to establish spatial boundary conditions, and they can not be considered as real CNN cells.

### A. Statement 1

“The absolute value of the state variables of every cell in an ISR CNN is bounded.”

*Proof:* Using the definition of  $g_m(x^c)$  given in (2), one can separate the cell dynamic law for the linear and the two saturation regions,

$$\tau \frac{dx^c}{dt} = \begin{cases} -mx^c + m - 1 + \sum_{d \in N(c)} a_d^c y^d + k^c & ; \quad x^c > 1 \\ -x^c + \sum_{d \in N(c)} a_d^c y^d + k^c & ; \quad |x^c| \leq 1 \\ -mx^c + 1 - m + \sum_{d \in N(c)} a_d^c y^d + k^c & ; \quad x^c < -1 \end{cases} \quad (8)$$

These differential equations can be solved using conventional methods to yield,

$$x^c(t) = x^c(0)e^{-\frac{m}{\tau}t} + \frac{1}{\tau} \int_0^t \left[ m - 1 + \sum_{d \in N(c)} a_d^c y^d(\theta) + k^c \right] e^{-\frac{m}{\tau}(t-\theta)} d\theta \quad ; \quad x^c > 1 \quad (9)$$

$$x^c(t) = x^c(0)e^{-\frac{t}{\tau}} + \frac{1}{\tau} \int_0^t \left[ \sum_{d \in N(c)} a_d^c y^d(\theta) + k^c \right] e^{-\frac{t-\theta}{\tau}} d\theta \quad ; \quad |x^c| \leq 1 \quad (10)$$

$$x^c(t) = x^c(0)e^{-\frac{m}{\tau}t} + \frac{1}{\tau} \int_0^t \left[ 1 - m + \sum_{d \in N(c)} a_d^c y^d(\theta) + k^c \right] e^{-\frac{m}{\tau}(t-\theta)} d\theta \quad ; \quad x^c < -1 \quad (11)$$

For these equations to be valid the time variable must be shifted so that  $t = 0$  every time the state variable enters a different region, and the initial condition  $x^c(0)$  must be defined accordingly.

In general, the cell may go in and out of the linear and saturation regions several times during the CNN processing. We define intervals  $[t_{Li}, t'_{Li}]$ ,  $i=1, \dots, N$  and  $[t_{Sj}, t'_{Sj}]$ ,  $j=1, \dots, M$  within which the state variable is in the linear region or in some saturation region, respectively. The union of these intervals contains the complete transient evolution of the cell. Hence, we must consider different initial conditions  $x^c_{Li}(0) = x^c(t=t_{Li})$ ,  $i=1, \dots, N$ , and  $x^c_{Sj}(0) = x^c(t=t_{Sj})$ ,  $j=1, \dots, M$ , and the corresponding time-shifts to use equations (9) through (11). Note that generally  $|x^c_{Li}(0)| = |x^c_{Sj}(0)| = 1$ , with the possible exception of the real (unshifted time) initial condition  $x^c_0(0)$ , which affects either  $x^c_{L1}(0)$  or  $x^c_{S1}(0)$ . If  $|x^c_0(0)| < 1$ , then  $|x^c_{L1}(0)| = |x^c_0(0)| < 1$ , and if  $|x^c_0(0)| > 1$  then  $|x^c_{S1}(0)| = |x^c_0(0)| > 1$ . In any case, the initial conditions are all finite, and  $|x^c_{Li}(0)| \leq 1$ ,  $\forall i=1, 2, \dots, N$ , while  $|x^c_{Sj}(0)| \geq 1$ ,  $\forall j=1, 2, \dots, M$ .

Since the state variable must always be in one of the three regions, we only need to demonstrate that equations (9) through (11) are bounded. Using Schwartz's inequality several times on (9), taking into account that the output variables are  $|y^c(t)| \leq 1$  and that  $m \geq 1$ , obtains the following bounded result,

$$|x^c(t)| \leq \frac{m-1+M^c}{m} + \left[ |x^c(0)| - \frac{m-1+M^c}{m} \right] e^{-\frac{m}{\tau}t} \quad (12)$$

The same result is obtained from (11). Finally, a similar result can be obtained for the linear region using equation (10), or we can simply consider that by definition  $|x^c(t)| \leq 1$  in this region. Therefore, state variables are globally bounded.  $\square$

### B. Statement 2

“For any cell  $c$ , the minimum bound of the absolute value of equilibrium points is a bound for the state variable at any time instant, assuming that it is true at  $t = 0$ .”

*Proof:* Let us first obtain a value for the bound of the state variables. From (12), which is valid for either saturated region, we can obtain a bound for the state variable in each interval  $[t_{S_j}, t'_{S_j})$ . We define function  $B_{S_j}^c(t)$  as the right-hand side of (12), which is a time dependent bound for the state variable within interval  $[t_{S_j}, t'_{S_j})$ . Function  $B_{S_j}^c(t)$  can take only two different forms, illustrated in Fig. 6, which allow obtaining the following results,

$$\text{if } |x_{S_j}^c(0)| \leq \frac{m-1+M^c}{m} \quad \text{then } |x^c(t)| \leq B_{S_j}^c(\infty) = \frac{m-1+M^c}{m} \quad (13)$$

$$\text{if } |x_{S_j}^c(0)| > \frac{m-1+M^c}{m} \quad \text{then } |x^c(t)| \leq B_{S_j}^c(0) = |x_{S_j}^c(0)| \quad (14)$$

From which we can conclude that

$$|x^c(t)| \leq \max \left\{ \frac{m-1+M^c}{m}, |x_{S_j}^c(0)| \right\} \quad \forall t \in [t_{S_j}, t'_{S_j}), j = 1, \dots, M \quad (15)$$

Taking into account the possible values of  $|x_{S_j}^c(0)|$ , obtains the following result,

$$|x^c(t)| \leq \max \left\{ \frac{m-1+M^c}{m}, |x_0^c(0)| \right\} > 1 \quad \forall t \in \bigcup_{j=1}^M [t_{S_j}, t'_{S_j}) \quad (16)$$

The same procedure can be used for the linear region, or we may simply take into account that since  $|x^c(t)| \leq 1$ ,  $\forall t \in [t_{L_i}, t'_{L_i})$  for any  $i = 1, \dots, N$ , (16) can be extended to

$$|x^c(t)| \leq \max \left\{ \frac{m-1+M^c}{m}, |x_0^c(0)| \right\} \quad \forall t \geq 0 \quad (17)$$

Let us now determine the maximum possible absolute value of an equilibrium point. For this purpose, we look at the dynamic route of ISR cells considered as isolated, first-order dynamic systems (that is, considering the output of neighboring cells as time-invariant). Then, we can define

$$i^c \equiv \sum_{d \in N^c(c)} a_d^c y^d + k^c \quad (18)$$

which contains all the “time-invariant” contributions to the cell. Note that the summation extends to



the *reduced neighborhood*  $N'(c) = N(c) - \{c\}$  of the cell. Then, using this definition in (8), the dynamic route can be formulated as

$$\tau \frac{dx^c}{dt} = \begin{cases} -m(x^c - 1) - 1 + a_c^c y^c + i^c & ; \quad x^c > 1 \\ -x^c + a_c^c y^c + i^c & ; \quad |x^c| \leq 1 \\ -m(x^c + 1) + 1 + a_c^c y^c + i^c & ; \quad x^c < -1 \end{cases} \quad (19)$$

as depicted in Fig. 7. The value of the equilibrium points in each of the three regions above can be obtained making the derivative equal to zero in (19) and using the definition of  $y^c(x)$  given in (2), which yields,

$$x_1^c = \frac{m - 1 + a_c^c + i^c}{m} > 1 \quad x_2^c = \frac{-i^c}{a_c^c - 1}, \quad |x_2^c| \leq 1 \quad x_3^c = -\frac{m - 1 + a_c^c - i^c}{m} < -1 \quad (20)$$

where we have included the condition required for the equilibrium points to be “real”, rather than “virtual”. Using  $|y^c(t)| \leq 1$  in (18) we obtain the maximum possible absolute value of  $i^c$ ,

$$|i^c| \leq \sum_{d \in N'(c)} |a_d^c| + |k^c| \quad (21)$$

which, used in (20) or (20), obtains the maximum possible absolute value of a cell equilibrium point,

$$|x^c| \leq \frac{m - 1 + \sum_{d \in N(c)} |a_d^c| + |k^c|}{m} = \frac{m - 1 + M^c}{m} \quad (22)$$

The right-hand side of this equation coincides with that of (17) under the assumption made in this statement.  $\square$

### C. Statement 3

“There is a hyper-rectangular region around the origin of the state space that is a global attracting region.”

*Proof:* This hyper-rectangular region is defined by a set of intervals, one for each cell,

$$I^c = \left[ -\frac{m - 1 + M^c}{m}, \frac{m - 1 + M^c}{m} \right] \quad \forall c \in GD \quad (23)$$

From (13), if the state variable  $x^c$  of a cell belongs to  $I^c$  at a time instant (which may be redefined as  $t = 0$ ), then it will belong to  $I^c$  at any later instant. On the other hand, from (12) we have determined that,

$$\lim_{t \rightarrow \infty} |x^c(t)| \leq \frac{m - 1 + M^c}{m} \quad (24)$$

which shows that if the state variable of a cell is outside  $I^c$  at a time instant, the state variable will

either be in  $I^c$  or arbitrarily close to its borders after a sufficient amount of time.  $\square$

Fig. 8 illustrates this for the simple case of a two-cell network: if the state vector  $X = (x^1, x^2)$  of the network is outside the attracting region  $I^1 \times I^2$ , it evolves towards it; and if it is inside, it never escapes.

#### D. Statement 4

“ISR CNNs with central-feedback coefficients larger than unity ( $a_c^c > 1$ ) have no stable equilibrium points within the open hypercube  $(-1,1)^n$ .”

*Proof:* The slope of dynamic routes in the linear region is given as  $s = a_c^c - 1$ , which is positive in the cases considered. Hence, any equilibrium point in the linear region is unstable.  $\square$

Only stable equilibrium points can be reached in a real network due to noise and perturbations. Hence, if a real network with ( $a_c^c > 1$ ) converges, its output is binary.

#### E. Statement 5

“ISR CNNs with reciprocal feedback templates are convergent.”

*Proof:* The demonstration is identical to that employed by Chua and Yang in [7] for the original model. A CNN is said to be reciprocal if

$$a_d^c = a_c^d, \quad \forall c \in GD, \forall d \in GD \quad (25)$$

We will use the same “energy-function” proposed in [7]:

$$E(t) = \sum_{c \in GD} y^c(t) \left\{ -\frac{1}{2} \sum_{d \in GD} a_d^c y^d(t) + \frac{1}{2} y^c(t) - \sum_{d \in GD} b_d^c u^d - d^c \right\} \quad (26)$$

Since the output variables are restricted to the  $[-1,1]$  interval, this function is bounded for any set of finite CNN coefficients, boundary conditions, initial states, and input values. We will now demonstrate that it is a continuously decreasing function of time. For this purpose taking the time derivative of (26), changing variables ( $c$  for  $d$  and vice-versa) in one of the resulting sums, using the chain rule and using (25), we obtain<sup>7</sup>

$$\frac{dE(t)}{dt} = - \sum_{c \in GD} \left\{ \sum_{d \in GD} [a_d^c y^d + b_d^c u^d] + d^c - y^c \right\} \frac{dy^c}{dx^c} \frac{dx^c}{dt} \quad (27)$$

Then, taking into account the following three equations,

$$a_d^c = b_d^c = 0, \quad \forall d \notin N(c) \quad \frac{dy^c}{dx^c} = \begin{cases} 1, & \forall |x^c| \leq 1 \\ 0, & \forall |x^c| > 1 \end{cases} \quad y^c = x^c, \quad \forall |x^c| \leq 1 \quad (28)$$

(27) can be transformed into,

7. The problem of the discontinuity in the derivative of the output variable can be avoided as described in [7], and will not be treated here. In circuit implementations, the discontinuity will not exist.

$$\frac{dE(t)}{dt} = - \sum_{\substack{c \in GD \\ |x^c| \leq 1}} \left\{ -x^c + \sum_{d \in N(c)} [a_d^c y^d + b_d^c u^d] + d^c \right\} \frac{dx^c}{dt} \quad (29)$$

Since only the cells whose state variables are in the linear region are included in the sum,  $g_m(x^c) = x^c$ ; and (1) can be used in the above equation to obtain

$$\frac{dE(t)}{dt} = -\frac{1}{\tau} \sum_{\substack{c \in GD \\ |x^c| \leq 1}} \left[ \frac{dx^c}{dt} \right]^2 \leq 0 \quad (30)$$

which demonstrates that  $E(t)$  is a monotonically decreasing function of time. Now (30) can be changed using the last two equations in (28) as follows,

$$\frac{dE(t)}{dt} = -\frac{1}{\tau} \sum_{\substack{c \in GD \\ |x^c| \leq 1}} \left[ \frac{dx^c}{dt} \right]^2 = -\frac{1}{\tau} \sum_{\substack{c \in GD \\ |x^c| \leq 1}} \left[ \frac{dy^c}{dt} \right]^2 = -\frac{1}{\tau} \sum_{c \in GD} \left[ \frac{dy^c}{dt} \right]^2 \leq 0 \quad (31)$$

Since  $E(t)$  is a bounded and monotonic decreasing function of time, its limit for  $t \rightarrow \infty$  exists and therefore, the limit of its derivative must be zero,

$$\lim_{t \rightarrow \infty} \frac{dE(t)}{dt} = 0 \quad \Rightarrow \quad \lim_{t \rightarrow \infty} \sum_{c \in GD} \left[ \frac{dy^c}{dt} \right]^2 = 0 \quad \Rightarrow \quad \lim_{t \rightarrow \infty} \frac{dy^c}{dt} = 0, \forall c \in GD \quad (32)$$

where (31) has been used and the fact that if a sum of positive summands is zero, every summand is zero. The final result in (32) demonstrates that all output variables converge.  $\square$

Once the output variables are stable, every individual cell can be considered as an isolated, first-order nonlinear system. The resulting dynamic-routes shown in Fig. 7 can be used to demonstrate that the state variables also converge. However, it is interesting to obtain a formal demonstration to provide expressions for the value of the equilibrium points of the state variables as a function of the output variables. For this purpose, we define

$$r^c(t) \equiv \sum_{d \in N(c)} a_d^c y^d(t) + k^c \quad (33)$$

and

$$R^c \equiv \lim_{t \rightarrow \infty} r^c(t) = \sum_{d \in N(c)} a_d^c \lim_{t \rightarrow \infty} y^d(t) + k^c \quad (34)$$

which exists since the limits of all output variables exist. Note that once the output variables have converged, the state variables of the cells are confined to one of the three regions. If the state variable of a particular cell is in the upper saturated region we can use (9), rewritten using the previous definitions, as follows

$$\begin{aligned}
\lim_{t \rightarrow \infty} x^c(t) &= \lim_{t \rightarrow \infty} x^c(0) e^{-\frac{m t}{\tau}} + \frac{1}{\tau} \lim_{t \rightarrow \infty} e^{-\frac{m t}{\tau}} \int_0^t [m - 1 + r^c(\theta)] e^{\frac{m \theta}{\tau}} d\theta = \\
&= \frac{1}{\tau} \lim_{t \rightarrow \infty} \frac{\int_0^t [m - 1 + r^c(\theta)] e^{\frac{m \theta}{\tau}} d\theta}{e^{\frac{m t}{\tau}}} = \frac{1}{m} \lim_{t \rightarrow \infty} \frac{[m - 1 + r^c(t)] e^{\frac{m t}{\tau}}}{e^{\frac{m t}{\tau}}} = \frac{m - 1 + R^c}{m}
\end{aligned} \tag{35}$$

where we have used the rule of L'Hôpital. If the state variable is in the lower saturated region we can use the same procedure starting from (11), which yields,

$$\lim_{t \rightarrow \infty} x^c(t) = \frac{1 - m + R^c}{m} \tag{36}$$

Finally, if the state variable is in the linear region, we can use (10) in the same manner,

$$\begin{aligned}
\lim_{t \rightarrow \infty} x^c(t) &= \lim_{t \rightarrow \infty} x^c(0) e^{-\frac{t}{\tau}} + \frac{1}{\tau} \lim_{t \rightarrow \infty} e^{-\frac{t}{\tau}} \int_0^t r^c(\theta) e^{\frac{\theta}{\tau}} d\theta = \\
&= \frac{1}{\tau} \lim_{t \rightarrow \infty} \frac{\int_0^t r^c(\theta) e^{\frac{\theta}{\tau}} d\theta}{e^{\frac{t}{\tau}}} = \lim_{t \rightarrow \infty} \frac{r^c(t) e^{\frac{t}{\tau}}}{e^{\frac{t}{\tau}}} = R^c
\end{aligned} \tag{37}$$

The above expressions can be used to determine the set of possible equilibrium points by considering all the possible combinations of binary output for the cells in a neighborhood (for convergent CNNs with  $a_c^c > 1$ ), as done in [10]. For this purpose, it must be taken into account that equations (35) through (37) are only valid when the results are consistent with the region for which they were obtained. The stability of the equilibrium points can then be observed from the derivative of the state variables at the equilibrium points, given by (1).

#### F. Statement 6

“For any two models in the ISR family, there is a one-to-one correspondence between their sets of network equilibrium points which preserves the local stability and the value of the output vector”

*Proof:* We will use matrix notation in the following. For this purpose, we assume a network with  $N$  inner cells, and define vectors  $X$ ,  $Y$ ,  $U$ , and  $D$  as  $N \times 1$  matrices with their individual components  $x^c$ ,  $y^c$ ,  $u^c$ , and  $d^c$  in some arbitrary order. We also define two  $N \times N$  matrices  $A$  and  $B$  with elements given respectively by  $a(c, d) = a_d^c$  and  $b(c, d) = b_d^c$  for  $c, d = 1, \dots, N$ , and two  $N \times 1$  vectorial functions  $F(X)$  and  $G_m(X)$  with individual components given by  $f(x^c)$  and  $g_m(x^c)$  as defined in (2). Equation (1) can then be written for the whole network as

$$\frac{1}{\tau} \frac{dX}{dt} = -G_m(X) + AY + BU + D \tag{38}$$

and equation (2) as

$$Y = F(X) \quad (39)$$

As previously stated, boundary conditions can be included in (38) by redefining the elements of the offset term vector  $D$  associated to border cells.

We now focus attention on function  $g_m(x)$ , defined in (2) and plotted in Fig. 5 for an arbitrary  $m \in [1, \infty)$ . Let us consider a map  $w = g_m(x)$ . Since  $g_m(x)$  is a monotonically increasing function, it is invertible. Note also that both the image and the domain of this function equal the complete real axis  $\mathfrak{R}$ . Hence, both  $g_m(x)$  and  $g_m^{-1}(w)$  are one-to-one and defined anywhere in  $\mathfrak{R}$ . From Fig. 5 and equation (2), we can obtain the following expression for  $g_m^{-1}(x)$

$$g_m^{-1}(w) = \begin{cases} 1 + \frac{w-1}{m} & , \text{ if } w > 1 \\ w & , \text{ if } |w| < 1 \\ -1 + \frac{w+1}{m} & , \text{ if } w < -1 \end{cases} \quad (40)$$

which is also monotonically increasing. From Fig. 5, we also have that

$$\left[ x > 1 \Leftrightarrow w > 1 \right] \quad \left[ |x| \leq 1 \Leftrightarrow |w| \leq 1 \right] \quad \left[ x < -1 \Leftrightarrow w < -1 \right] \quad (41)$$

which means that both  $g_m(x)$  and  $g_m^{-1}(w)$  preserve the region (upper-saturated, linear, or lower-saturated) of their variable.

These results can be extended to the vectorial form considering a pair of inverse maps,  $W = G_m(X)$  and  $X = G_m^{-1}(W)$ , which are both one-to-one, defined on the entire space  $\mathfrak{R}^N$  and preserve the output vector,

$$\begin{aligned} W = G_m(X) & \Rightarrow F(W) = F(X) = Y \\ X = G_m^{-1}(W) & \Rightarrow F(X) = F(W) = Y \end{aligned} \quad (42)$$

Note that preservation of the output vector is independent of the value of parameter  $m$ .

Consider now a CNN designed for a specific application, with a particular value of parameter  $m$ . For any input vector  $U$  the set of equilibrium points of the network can be obtained from (40) by requesting that the derivative of the state vector  $X$  be null,

$$G_m(X) = AY + BU + D \quad (43)$$

The solution of this equation gives the set of equilibrium points of the network  $\{X_i\}$ . We then define the corresponding set  $\{W_i\} = \{G_m(X_i)\}$ . From the equilibrium point condition in (43), it is clear that

$$\{W_i\} = \{AY_i + BU + D\} \quad (44)$$

where  $\{Y_i\} = \{F(X_i)\}$ . Let us now consider another CNN, identical to the previous one, with the exception of the value of parameter  $m$ , denoted now  $m'$ , and with the same input vector  $U$ . For each

equilibrium point  $X_i$  in the previous network, we define a point  $X'_i$  in the state space of the new network given by,

$$X'_i = G_m^{-1}(G_m(X_i)) = G_m^{-1}(W_i) \quad (45)$$

Given the preservation of the output vector in both  $G_m(X_i)$  and  $G_m^{-1}(W_i)$  we have,

$$Y'_i = F(X'_i) = F(W_i) = F(X_i) = Y_i \quad (46)$$

Using this in (44), we obtain

$$W_i = AY'_i + BU + D \quad (47)$$

This can finally be used in (45) to obtain,

$$X'_i = G_m^{-1}(AY'_i + BU + D) \quad (48)$$

or in a different form,

$$G_m(X'_i) = AY'_i + BU + D \quad (49)$$

which means that points  $X'_i$  are equilibrium points of the new network.

The correspondence between the two sets  $\{X'_i\}$  and  $\{X_i\}$  is one-to-one and hence, the new network has the same or a larger number of equilibrium points than the previous one. However, since this process can be repeated by swapping the roles of the two networks, the only possible result is that the two networks have the same number of equilibrium points. Hence,  $\{X'_i\}$  and  $\{X_i\}$  represent the sets of equilibrium points of the two networks, and equation (45) defines a one-to-one correspondence between them which, as seen from (46), preserves the output vector. We will now demonstrate that this correspondence preserves the local stability properties as well.

Consider again a generic value of parameter  $m \in [1, \infty)$ . For each input vector  $U$  (assumed time-invariant), equation (38) defines an autonomous system which can be formulated as

$$\frac{1}{\tau} \frac{dX}{dt} = V(X) \quad (50)$$

with

$$V(X) = -G_m(X) + AY + BU + D \quad (51)$$

The set of equilibrium points of (50) has been denoted previously as  $\{X_i\}$ . Their local-stability properties can be determined from the real-part sign of the eigenvalues of the  $N \times N$  matrix  $J(V)|_{X_i}$  resulting from the linearization of (50) around each equilibrium point  $X_i$  [13], [14],

$$\frac{1}{\tau} \frac{dX}{dt} = J(V)|_{X_i} \cdot (X - X_i) \quad (52)$$

where  $J(V)|_{X_i}$  is defined by

$$j(c, d)|_{X_i} = \left. \frac{\partial v^c}{\partial x^d} \right|_{X_i} \quad (53)$$

Clearly, since  $BU + D$  is independent of  $X$ ,

$$J(V)|_{X_i} = -J(G_m(X))|_{X_i} + A \cdot J(Y(X))|_{X_i} \quad (54)$$

Matrices  $J(G_m(X))|_{X_i}$  and  $J(Y(X))|_{X_i}$  are both diagonal since the individual elements of  $G_m(X)$  and  $Y(X)$  depend only on the corresponding individual element of  $X$ , that is,  $g_m^c(X) = g_m^c(x^c)$  and  $y^c(X) = y^c(x^c)$ . The diagonal elements of both matrices can be obtained from (2),

$$\left. \frac{\partial g_m^c}{\partial x^c} \right|_{X_i} = \begin{cases} m & \text{;if } |x^c| > 1 \\ 1 & \text{;if } |x^c| \leq 1 \end{cases} \quad ; \quad \left. \frac{\partial y^c}{\partial x^c} \right|_{X_i} = \begin{cases} 0 & \text{;if } |x^c| > 1 \\ 1 & \text{;if } |x^c| \leq 1 \end{cases} \quad (55)$$

Now consider two CNN systems, identical except for their values of parameter  $m$ . As shown previously, the two corresponding sets of equilibrium points are related one-to-one, and the output vector is preserved. Hence, for any pair of related equilibrium points of these two systems the second summand  $A \cdot J(Y(X))|_{X_i}$  in (54) is invariant. Therefore, differences between their corresponding  $J(V)|_{X_i}$  matrices can only be originated by the first summand  $-J(G_m(X))|_{X_i}$  in (54), which is a diagonal matrix. Also, from (55), differences appear only in diagonal elements corresponding to saturated cells. On the other hand, from (55), columns of  $A \cdot J(Y(X))|_{X_i}$  corresponding to saturated cells have all zero element, and therefore, in the  $J(V)|_{X_i}$  matrices all elements in columns corresponding to saturated cells are zero, except that in the diagonal which is given by  $-m$ . These diagonal elements are hence eigenvalues, all equal to  $-m$ . The remaining eigenvalues can be obtained from the submatrix resulting from the elimination of the rows and columns corresponding to saturated cells. Since the  $J(V)|_{X_i}$  matrices of the two systems are identical except in the diagonal elements corresponding to saturated cells, this process leaves identical submatrices for the two systems, therefore with identical eigenvalues. In summary, eigenvalues corresponding to cells in the linear region are identical in the two systems, while those corresponding to saturated cells are always negative. Therefore, the stability of the equilibrium points is preserved.  $\square$

#### IV. THE FSR LIMIT

The statements in the previous section are valid for any value of  $m$  in the range  $m \in [1, \infty)$  which includes the Chua-Yang ( $m = 1$ ) and the FSR ( $m \rightarrow \infty$ ) models. In this last case, we can also make the following statement,

##### A. Statement 7

“In the FSR limit ( $m \rightarrow \infty$ ), the state vector is limited to the  $[-1, 1]^n$  hypercube independently of the particular CNN coefficients, assuming that the initial-state vector is within this hypercube.”

*Proof:* Simply note that

$$\lim_{m \rightarrow \infty} \frac{m-1+M^c}{m} = 1 \quad (56)$$

and therefore, using (23),

$$\lim_{m \rightarrow \infty} I^c = [-1, 1] \quad (57)$$

which demonstrates that the  $[-1,1]^n$  hypercube is a global attracting region.  $\square$

Also note that the state vector is attracted to this hypercube, if it is initially outside.

### B. FSR model formulation

Let us assume that the state vector of an FSR CNN is  $X(0) \in [-1,1]^n$ . Since in this model  $x^c \equiv y^c$  the cell equation for  $|x^c| < 1$ , can be modified as follows,

$$\tau \frac{dx^c}{dt} = -x^c + \sum_{d \in N(c)} a_d^c x^d + \sum_{d \in N(c)} b_d^c u^d + d^c \quad (58)$$

On the other hand, the state variable must be forced to remain in the unitary interval  $[-1,1]$  using a hard limiter, as illustrated in Fig. 3. The high slope (ideally infinite) of the external segments of  $g_m(x^c)$  ensures that the derivative of the state variable is null at  $|x^c| = 1$ , positive (ideally  $\infty$ ) for  $x^c < -1$  and negative (ideally  $-\infty$ ) for  $x^c > 1$ . In summary, the FSR cell model can be practically described by the following equation,

$$\tau \frac{dx^c}{dt} = \begin{cases} \sum_{d \in N(c)} a_d^c x^d + \sum_{d \in N(c)} b_d^c u^d + d^c & , \forall |x^c| < 1 \\ 0 & , \forall |x^c| = 1 \\ -\text{sgn}(x^c)\infty & , \forall |x^c| > 1 \end{cases} \quad (59)$$

Hence, the stability of the equilibrium points at  $|x^c| = 1$  depends on the sign of the lateral derivatives. Deviations towards the outside of  $[-1,1]$  are rapidly restored to the interval by the extreme values of the derivative at  $|x^c| > 1$ . On the other hand, deviations towards the inside of the interval will be increased or restored depending on the sign of the upper expression in (59), which coincides with the definition of  $h^c$  in (5) after performing the substitution  $x^c = z^c$ . Taking into account that in a real system the state variables will always fluctuate around any equilibrium point due to the presence of electrical noise and other perturbations (allowing it to escape from unstable equilibrium points), equation (59) can be considered identical to (4).

It is important to mention that, in real implementations  $m$  will always be finite. Nevertheless, for sufficiently high values of  $m$ , the properties of the CNN will be arbitrarily similar to that of the FSR model.

### C. Functionality of FSR CNNs

Previous sections describe and analyze a modification of the continuous-time CNN model,



resulting in simpler circuit implementations, which allows the integration of a higher number of cells in a single IC. Stability and convergence properties of the modified model have been shown to be similar to those of the original model. However, to take advantage of the many applications reported in literature for the original model, the I/O mapping of the CNN should be preserved after performing the modification of the model.

Statement 6 ensures preservation of the local stability properties of the system, since the Chua-Yang and FSR models are particular cases of the ISR model family. However, the basins of attraction of the different stable equilibrium points will be modified by the different dynamics of the two systems. Nevertheless, numerical experiments show that for most reported applications, the CNN model can be changed from the original to the FSR (in fact an ISR algorithm with  $m \gg 1$ ) without appreciable effects on the I/O mapping. This is particularly true in the case of early CNN applications, designed mainly by inspection of the stability properties of equilibrium points as a function of template coefficients [8], [15], [16]. Tab. 1 illustrates some numerical examples of image-processing with the original and the FSR CNN models. It can be observed that the resulting output image is the same. Note that the time required to converge to the final output (normalized to the time constant  $\tau$  of the network) is about half for the FSR algorithm. This is a positive consequence of eliminating the inertia of saturated state-variables to remain in the saturation region.

It can also be shown that uniform (proportional) variations of the templates and offset coefficients in (59) only affect the time constant of the network. For the original model, the same result is obtained if the loss term is influenced by the same proportional variation. However, the different signal ranges required for the state and output variables usually force the use of different circuit blocks to implement the loss term and the weighted output, resulting in non-uniform variations. Hence, another positive feature of the FSR model is its increased robustness against uniform variations of the CNN coefficients. This is important in aVLSI context, where process parameters are always subject to variations.

## V. SUMMARY

This paper describes and analyzes a modified continuous-time CNN model which results in more efficient circuit implementations and preserves most of the functionality of the original model. Stability results include those reported for the original CNN model in [7] and [8], and can be summarized as follows:

- State variables are bounded.
- The bound of the state variable coincides with the maximum value of an equilibrium point.
- There is a global attracting region.
- Convergence of reciprocal-feedback CNNs.
- Binary output of convergent CNNs with  $(a_c^c > 1)$ .

Except for the restrictions explicitly stated in the last two points, these results generally apply to any

feedback and control templates, offset terms, and boundary conditions (including non-uniform networks). They are also general for any set of initial states and cell input (not restricted to the unitary interval).

Other results in this paper were obtained to show the similarity between the modified and the original model. This includes the one-to-one correspondence of equilibrium points which preserves the output vector of the network and the local stability. Numerical examples are also used to show the invariance of I/O mapping between the two models.

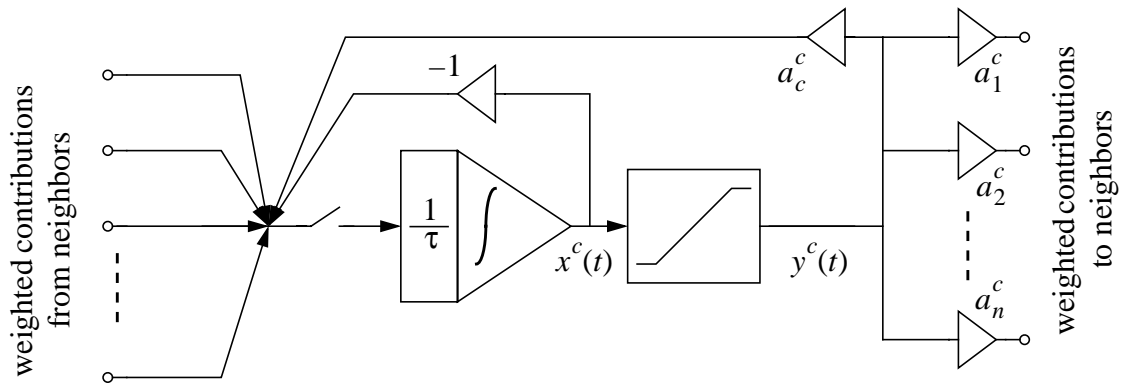
From an electronic implementation point of view, the modified model presents the following advantages:

- The state and output signals are merged into a single signal.
- The realization of the nonlinear function  $y(x)$  is not required.
- The normalized dynamic-range of all signals is  $\pm 1$ , and invariant with the application.
- The linear dissipative term is merged with the self feedback coefficient.
- Proportional variations of all coefficients have no effect on the I/O mapping of the network.
- Processing time is approximately halved in common applications.

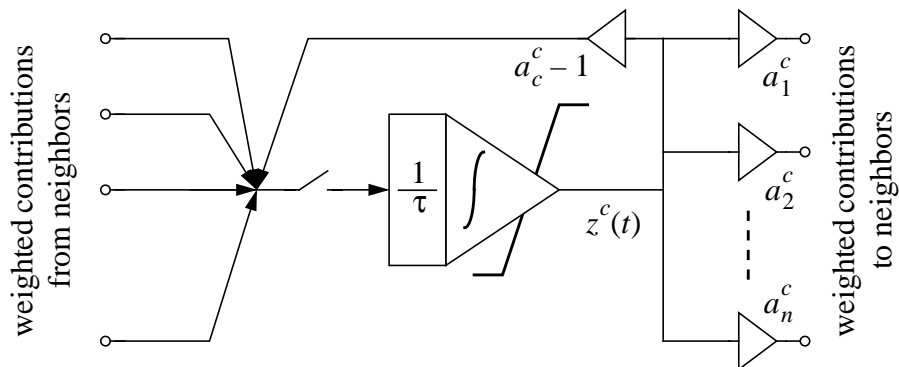
#### REFERENCES

- [1] E. Vittoz: "Analog VLSI Signal Processing: Why, Where and How?". *Analog Integrated Circuits and Signal Processing*, Vol. 6, pp. 27-44, July 1994.
- [2] J. Cruz: "A Fast, Complex and Efficient Test Implementation of the CNN Universal Machine". *Proc. of the 3<sup>rd</sup> Int. Workshop on Cellular Neural Networks and their Applications*, pp. 61-66. Rome, December 1994.
- [3] B.J. Sheu, S.H. Bang and W. Fang: "Analog VLSI Design of Cellular Neural Networks with Annealing Capability". *Proc. of the 3<sup>rd</sup> Int. Workshop on Cellular Neural Networks and their Applications*, pp. 387-392. Rome, December 1994.
- [4] P. Kinget and M. Steyaert: "A Programmable Analog Cellular Neural Network CMOS Chip for High-Speed Image Processing". *IEEE Journal of Solid-State Circuits*, Vol. 30, pp. 235-243, March 1995.
- [5] S. Espejo, A. Rodríguez-Vázquez and R. Domínguez-Castro: "Smart-Pixel Cellular Neural Networks in Analog Current-Mode CMOS Technology". *IEEE Journal of Solid-State Circuits*, Vol. 29, pp. 895-905, IEEE August 1994.
- [6] R. Domínguez-Castro, S. Espejo, A. Rodríguez-Vázquez, and R. Carmona: "A CNN Universal Chip in CMOS Technology". *Proc. of the 3<sup>rd</sup> Int. Workshop on Cellular Neural Networks and their Applications*, pp. 91-96. Rome, December 1994.
- [7] L.O. Chua and L. Yang: "Cellular Neural Networks: Theory". *IEEE Trans. Circuits and Systems*, Vol. 35, pp 1257-1272, October 1988.
- [8] L.O. Chua and L. Yang: "Cellular Neural Networks: Applications". *IEEE Trans. Circuits and Systems*, Vol. 35, pp 1273-1290, October 1988.
- [9] A. Rodríguez-Vázquez, S. Espejo, R. Domínguez-Castro, J.L. Huertas and E. Sánchez-Sinencio: "Current-Mode Techniques for the Implementation of Continuous- and Discrete-Time Cellular Neural networks", *IEEE Trans. Circuits and Systems-II*, Vol. 40, pp 132-146, March 1993.
- [10] J.A. Nossek, G. Seiler, T. Roska and L.O. Chua: "Cellular Neural Networks: Theory and Circuit Design". *Int. J. Circuit Theory and Applications*, Vol. 20, pp 533-553, John Wiley & Sons, September-October 1992.

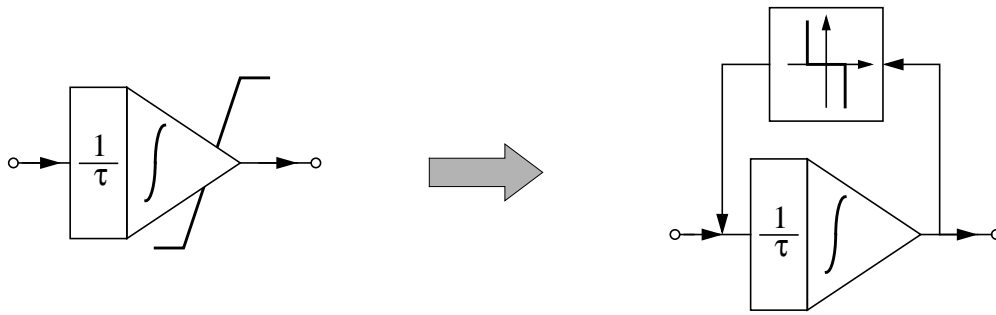
- [11] “CNN Analogic (dual) Software Library, Version 4.1”. Internal Report DNS-1-1993, Computer and Automation Institute, Hungarian Academy of Science, January 1993.
- [12] S. Espejo: “*VLSI Design and Modeling of CNNs*”. Ph. Dissertation, University of Sevilla, March 1994.
- [13] P.A. Cook: “*Nonlinear Dynamical Systems*”. Prentice/Hall International, 1986.
- [14] T.E. Stern: “*Theory of Nonlinear Networks and Systems, An Introduction*”. Addison-Wesley, Reading, Massachusetts, 1965.
- [15] T. Matsumoto, L.O. Chua and R. Furukawa: “CNN Cloning Template: Hole Filler”. *IEEE Trans. Circuits and Systems*, Vol. 37, pp 633-635, May 1990.
- [16] T. Matsumoto, L.O. Chua and H. Suzuki: “CNN Cloning Template: Connected Component Detector”. *IEEE Trans. Circuits and Systems*, Vol. 37, pp 635-638, May 1990.
- [17] S. Espejo, A. Rodríguez-Vázquez, R. Domínguez-Castro, and R. Carmona: “Convergence and Stability of the FSR CNN Model”. *Proceedings of the 3<sup>rd</sup> International Workshop on Cellular Neural Networks and their Applications*, pp. 411-416. Rome, December 1994.



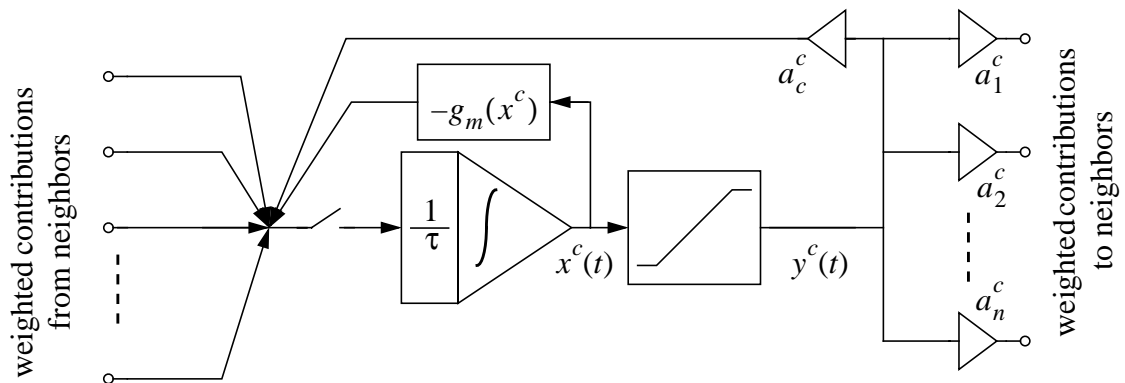
**Fig. 1.** Block diagram of a CT CNN cell circuitry according to the original cell model. Control template and offset-term implementation are not shown.



**Fig. 2.** Block diagram of CT CNN cell circuitry using the FSR model.



**Fig. 3. Realization of an integrator with saturation.**



**Fig. 4. Block diagram of ISR CNN cell circuitry.**

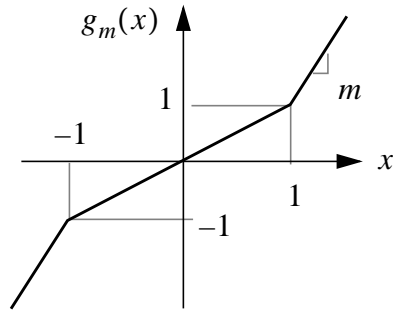


Fig. 5. Piece-wise linear loss term used in the ISR models.

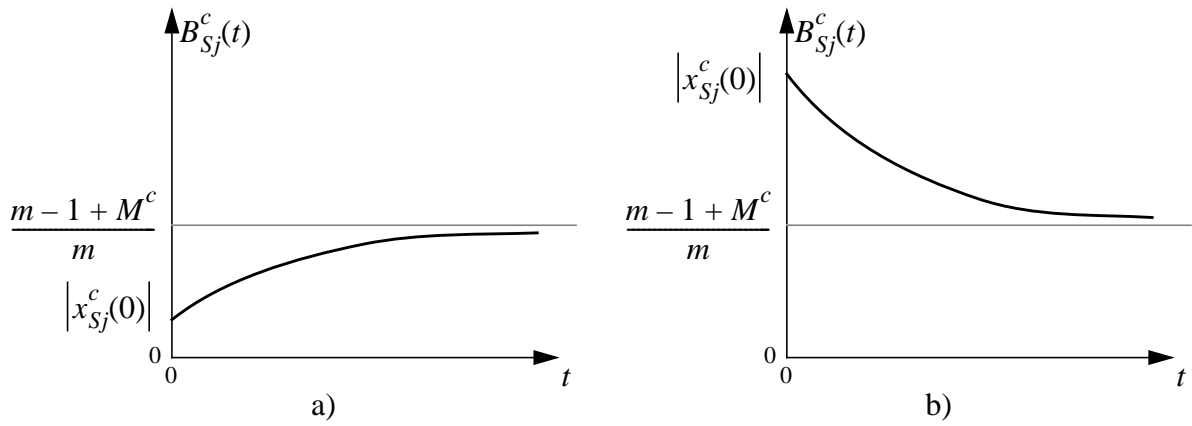
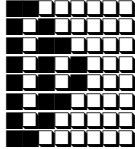
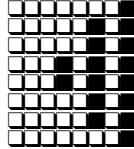
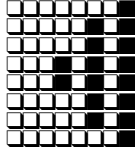
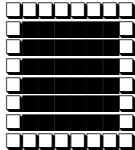
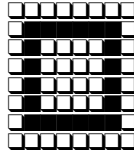
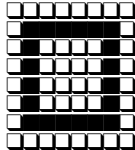
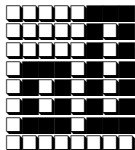
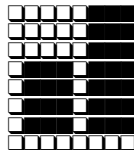

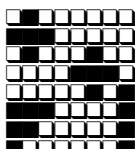

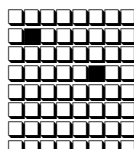
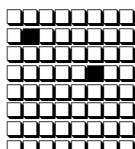


Fig. 6. Two possible forms of  $B_{S_j}^c(t)$ : a) case considered in (13), b) case considered in (14).



Table 1: Some processing examples with the original and the FSR CNN models.

APPLICATION	INPUT IMAGE	CHUA-YANG		FSR (m=100)	
		OUTPUT	Time ( $\tau$ )	OUTPUT	Time ( $\tau$ )
CONNECTED COMPONENT DETECTOR [16]			17.672		9.099
EDGES DETECTOR [8]			13.483		5.171
HOLE FILER [15]			7.326		3.100
DETECT SPEC. PATTERN [11]	 		6.531		2.101



## FIGURE AND TABLE CAPTIONS

- Fig. 1.** Block diagram of a CT CNN cell circuitry according to the original cell model. Control template and offset-term implementation are not shown.
- Fig. 2.** Block diagram of CT CNN cell circuitry using the FSR model.
- Fig. 3.** Realization of an integrator with saturation.
- Fig. 4.** Block diagram of ISR CNN cell circuitry.
- Fig. 5.** Piece-wise linear loss term used in the ISR models.
- Fig. 6.** Two possible forms of  $B_{S_j}^c(t)$ : a) case considered in (13), b) case considered in (14).
- Fig. 7.** Dynamic route of an ISR CNN cell.
- Fig. 8.** State-space trajectories of an ISR CNN network and global attracting region.

**Table 1:** Some processing examples with the original and the FSR CNN models.